ACS OMEGA

Open Access

http://pubs.acs.org/journal/acsodf

Article

Infrared Free-Electron Laser: A Versatile Molecular Cutter for Analyzing Solid-State Biomacromolecules

Takayasu Kawasaki,* Atsushi Nagase, Ken Hayakawa, Fumitsuna Teshima, Kiyohisa Tanaka, Heishun Zen, Fumio Shishikura, Norihiro Sei, Takeshi Sakai, and Yasushi Hayakawa

Cite This: *ACS Omega* 2025, 10, 13860−13867

Read Online

ACCESS | Metrics & More | Article Recommendations | Supporting Information

ABSTRACT: Free-electron lasers that oscillate in the infrared (IR) range of 1000 (10 μm) to 4000 cm^{-1} (2.5 μm) were applied to irradiate solid-phase polysaccharides and aromatic biomacromolecules. Synchrotron radiation IR microscopy (SR-IRM) and electrospray ionization mass spectroscopy (ESI-MS) analyses showed that *N*-acetyl glucosamine was isolated from the powdered exoskeleton of crayfish by irradiation at 1020 cm^{-1} (9.8 μm), resonating with the C−O stretching mode (νC−O). Irradiation at 3448 cm^{-1} (2.9 μm), which is resonant with the O−H stretching vibration (νO−H) of sulfonated lignin, dissociates the aggregate state and releases coniferyl aldehyde substituted with sulfinate, as shown by scanning electron microscopy, terahertz-coherent edge radiation spectroscopy, SR-IRM, and ESI-MS. These vibrational excitation reactions proceed at room temperature in the absence of solvent. Current and previous studies have demonstrated that intense IR lasers can be used as versatile tools for unveiling the internal structures of persistent biomacromolecules.

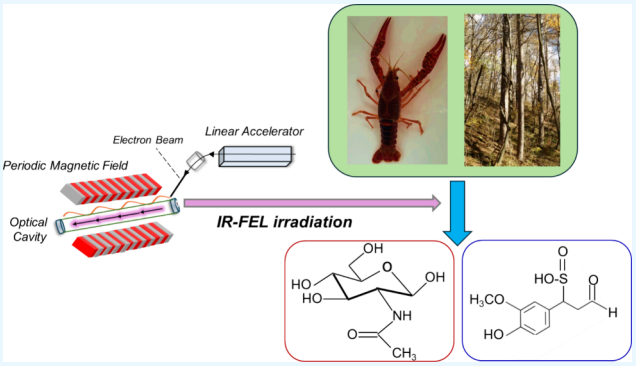

1. INTRODUCTION

Many types of biological and organic molecules give rise to mid- and near-infrared (IR) absorption bands from 1000 to 4000 cm^{-1} (= 2.5 to 10 μm), representing various stretching and bending vibrational modes (Figure 1). For example, C=O stretching, N−H bending, H−C−O bending, and O−H stretching vibrational modes appear at 1600−1800 cm^{-1} (5.5−6.0 μm), 1400−1600 cm^{-1} (6.0−7.0 μm), 1200−1300 cm^{-1} (≈7.5 μm), and 2500−3000 cm^{-1} (3.0−4.0 μm), respectively.[1−3]

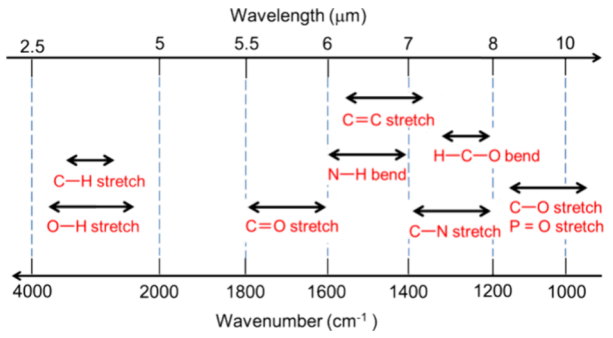

Figure 1. Various vibrational modes in the near- and mid-IR region from 1000 to 4000 cm^{-1} (below) and 2.5 to 10 μm (upper).

When vibrational excitation (VE) energy is applied to a molecule with a corresponding resonant wavelength, the chemical bond can be cleaved if the VE energy exceeds the bond energy. This phenomenon is known as IR multiphoton dissociation (IRMPD)[4−6] and can be caused by IR free-electron lasers (IR-FELs).[7−9] IR-FELs are accelerator-based picosecond-pulse lasers that can be oscillated by a strong interaction between a high-speed electron beam and synchrotron radiation generated in a periodic magnetic field (Figure 2).[10,11]

A remarkable feature of IR-FELs is their ability to excite vibrational modes with high photon density, which allows us to alter the chemical structure of various molecules in gas-phase chemicals, biological matter, and organic materials. In recent years, several experimental and theoretical studies using IR-FELs have been performed, including the ablation of biological tissues,[12,13] structural dynamics of biomolecules,[14−16] chemical reactions in the gas phase,[17] and spectroscopic imaging analyses.[18,19]

We tested the IR-FELs on several biomacromolecules, including peptide fibrils,[20] melanin pigments,[21] cellulose fibers,[22] and alkaline lignin.[23] These biopolymers were all

Received: August 15, 2024
Revised: March 14, 2025
Accepted: March 20, 2025
Published: April 2, 2025

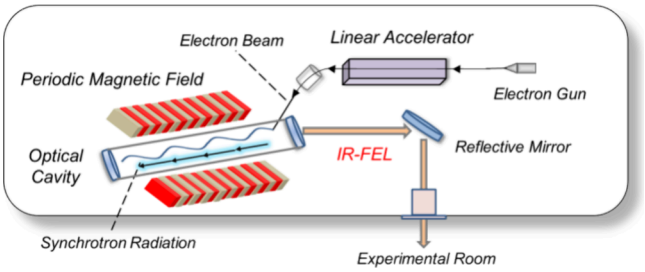

Figure 2. IR-FEL oscillation system. The system consists of three major parts: a linear accelerator, periodic magnetic field, and optical cavity. The IR-FEL beamline was transported through a reflective mirror to the laboratory in the experimental room.

degraded by mode-selective irradiations of the IR-FELs tuned to the specific wavelength of each compound under atmospheric conditions. The β-sheet stacking conformation of peptide fibril dissociates by the irradiation at amide I (6.1−6.2 μm),[20] melanin decomposes to release the pyrrole ring by irradiation at 5.8 μm (νC = O),[21] cellulose fragments to produce low-molecular-weight oligosaccharides via two-step irradiations at 9.1 μm (νC−O) after 7.2 μm (δH−C−O) or 3.5 μm (νC−H),[22] and alkaline lignin is degraded by irradiation at 2.9 μm (νO−H) and 7.1 μm (νC = C, νC−C).[23]

Here, we expanded the applicability of IR-FELs to other biomacromolecules to demonstrate the versatility of intense IR lasers in decomposing persistent biomacromolecules. Chitin is the main component of the outer shell of crustaceans, and its tough polymeric structure is composed of *N*-acetylglucosamine residues.[24,25] Sulfonated lignin (SL) is a waste material produced before alkaline treatment during industrial pulp preparation.[26,27] For chitin degradation, enzyme-mediated hydrolysis of glycoside bonds and various bacteria are known to degrade the carbohydrate structure.[28−30] To decompose lignin, metabolic enzymes in microorganisms and chemical degradation using organic peroxides and ionic liquids have recently been developed.[31−34] In this study, we demonstrate a unique approach using a linear accelerator distinct from biological systems or chemical catalysis.

2. MATERIALS AND METHODS

2.1. Materials. Shrimp shell chitin was purchased from Sigma-Aldrich (St. Louis, MO, USA). *N*-Acetyl-D(+)-glucosamine was purchased from FUJIFILM Wako Pure Chemical Corporation (Osaka, Japan). Crayfish exoskeletons were prepared as follows: Adult crayfish (*Procambarus clarkii*) were collected from local ponds and maintained in separate plastic containers under a dark/light cycle of 12 h/12 h, and fresh water was changed during feeding. Five molting shells were collected and stored at − 25 °C in a refrigerator until use. SL was obtained from Tokyo Chemical Industry Co., Ltd. (Tokyo, Japan). It is primarily produced from wood via sodium sulfite treatment.

2.2. IR-FEL Irradiation Systems. We used the KU-FEL at Kyoto University for mid-IR FEL (MIR-FEL) at 7.1 and 9.8 μm,[35,36] and the FEL oscillation system at Nihon University (LEBRA-FEL) was employed for near-infrared FEL (NIR-FEL) at 2.9 and 5.0 μm.[37,38] The oscillation system and irradiation setup are described in detail in the Supporting Information (Figures S1 and S2). The laser power ranged from 5 to 25 mJ, and the beam diameter was set to approximately 200−400 μm above the sample surface by using a parabolic mirror for MIR-FEL and a focusing lens made of CaF_2 (f = 100 mm) for NIR-FEL. To irradiate the outer shell of the crayfish, one solid arm was mashed in a mortar, and the resulting powder (ca. 50 mg) was placed in a 5 mL triangular flask (Figure 3A). For SL, the sample powder (5−10 mg) was added

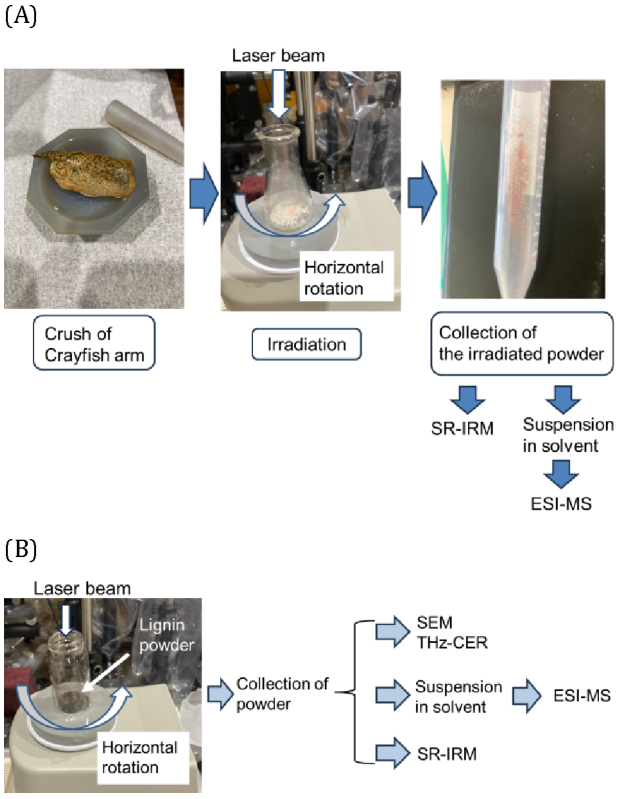

Figure 3. Experimental scheme from sample preparation to structural analysis. (A) Crayfish arms. (B) SL.

to a glass column (2 cm in diameter and 5 cm in length) (Figure 3B). In both cases, the IR-FEL was irradiated vertically for 10 min at room temperature. The sample bottle was shaken horizontally several times to allow the radiative energy to penetrate the powder.

2.3. Synchrotron Radiation-Infrared Microscopy (SR-IRM). BL6B synchrotron radiation-based IR microscopy was used at the UVSOR.[39] The instrument was composed of an IRT-7000 IR microscope combined with an FT/IR-6100 series spectrometer (Jasco Co.), which covers the wavenumber range of 350−15,000 cm^{-1} (45 meV−1.8 eV). The mid-IR spectra were measured using a Michelson-type interferometer in reflection mode and scanning 128 times. The sample powder (≈10 mg) was suspended in water (1 mL), and the mixture (20 μL) was placed on a metal coating plate. After drying, the plates were placed on a horizontally mutable stage. Observations were made using a 16 × Cassegrain lens with an aperture of 50 μm × 50 μm. The IR spectra were recorded from 700 to 4000 cm^{-1}.

2.4. Liquid Chromatography Electrospray Ionization Mass Spectroscopy (ESI-MS). A Prominence LXQ instrument (Shimadzu Thermo Fisher Scientific, Kyoto, Japan) was used. The mass chromatography condition was as follows: For chromatography, a sugar-D column (Nacalai Tesque, Kyoto, Japan) with dimensions of 4.6 × 150 mm and particle size of 5.0 μm was used. The elution was performed using 20% water

https://doi.org/10.1021/acsomega.4c07531
ACS Omega 2025, 10, 13860−13867

and 80% acetonitrile. The flow rate was 1.0 mL/min, the column temperature was 30 °C, and the sample size was 10 μL. The MS spectrum was acquired with the following parameters: electrospray voltage, 6.0 kV; temperature of ion transfer tube, 320 °C; and mass range of 100−2000 m/z. Sample powders were suspended in a 20% water and 80% acetonitrile solution and filtered using DISMIC-13HP (0.45 μm pore size, ADVANTEC, Co.) before injection into the column device.

2.5. Scanning Electron Microscopy (SEM) Observation. A Miniscope TM3000 (Hitachi High-Tech Co., Tokyo, Japan) was used in this study. The SL powder was placed on carbon tape and injected into a vacuum chamber. The acceleration voltage was set at 5.0 kV.

2.6. Terahertz Coherent Edge Radiation (THz-CER) Spectroscopy. We developed various coherent radiation sources at the LEBRA at Nihon University.[40−42] In this light source, the electron bunch length can be shortened to several tens μm, and powerful optical pulses can be obtained in the sub-THz-to-THz frequency region. CER is generated from a downstream bending magnet in the straight section of a parametric X-ray to an experimental room, and the CER beam can be used for various applied experiments in the THz region. The details are described in the Supporting Information (Figures S3 and S4). Samples were prepared by cutting a hole (1 cm in diameter) on a thick paper (ca. 0.2−0.3 mm in thickness) and placing SL powder (ca. 20 mg) on a horizontal plate in the hole. The paper was pressed from above using a pelleting machine, and the resulting minidisk was fixed to a sample holder that was set vertically against the THz beam.

3. RESULTS

3.1. Degradation of Chitin and Outer Shells of Crayfish. First, the chitin was irradiated. In Figure 4A, the C−O stretching mode (νC−O) in the glycoside bonds appears at 1005 cm^{-1} before irradiation (bottom) and 5.0 μm (2000 cm^{-1}) after irradiation, which is a low-absorption wavelength (middle). By contrast, the peak intensity diminished after irradiation at 9.8 μm (1020 cm^{-1}), which resonates with the C−O stretching mode, indicating that the number of glycoside bonds decreased after irradiation (upper). In Figure 4B, amide carbonyl stretching bands (νC = O) corresponding to the amide bond of *N*-acetyl glucosamine are located at 1617 and 1651 cm^{-1}, where the intensity of the latter peak increased slightly after 9.8 μm irradiation (upper) compared with that before irradiation (bottom) and after 5.0 μm irradiation (middle). These spectral changes indicate that the main chain of chitin was deformed by glycoside bond-targeting irradiation.

Next, the natural powder extracted from the outer shell of the crayfish was tested (Figure 5A−C).

The broad band from 1000 to 1200 cm^{-1} implies IR absorption of glycoside bonds (νC−O), and the intensity substantially decreased after irradiation at 9.8 μm (Figure 5A, red dotted square). This indicates that the C−O bonds in the natural components of crayfish were degraded by irradiation. In addition, the peaks at 1550 and 1650 cm^{-1} were clearly diminished after irradiation (red dotted lines). This region contains the N−H bending mode (δN−H) and C = O stretching mode (νC = O) of the *N*-acetylglucosamine residues. Therefore, it can be implied that part of the poly carbohydrate chain was cleaved, releasing the *N*-acetylglucosamine residues and decreasing the absorption intensities of the *N*-acetyl groups in the IR region.

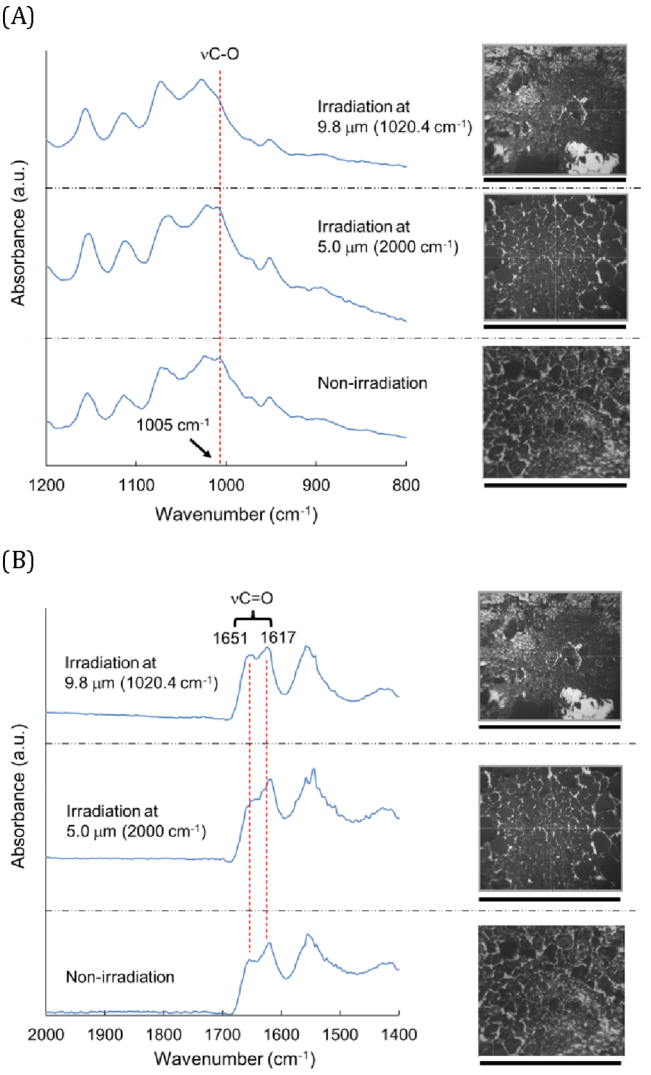

Figure 4. Irradiation effect of IR-FEL on chitin. (A) SR-IRM spectra of chitin before (bottom) and after irradiations at 9.8 μm (top) and 5.0 μm (middle) from 800 to 1200 cm^{-1}. The photographs on the right show microscopic images of the measurement area on the sample surface. Black bar: 1 mm. (B) SR-IRM spectra of chitin before (bottom) and after irradiations at 9.8 (upper) and 5.0 μm (middle) from 1400 to 2000 cm^{-1}. Photographs on the right are the same as those in (A).

These decompositions were further analyzed using ESI-MS (Figures 5B and 5C). We compared the chromatographic profiles after irradiation at 9.8 μm (blue) and 5.0 μm (red) (Figure 5B, left panel). The elution peak at 4.6 min increased more in the former case than the latter (dotted arrows at both ends), and the other peaks hardly changed. The elution time matches that of *N*-acetylglucosamine alone (right panel). In addition, mass chromatograms during the elution (15 min in total) showed that the mass peaks corresponding to 243 Da were more intense at 9.8 μm (blue) than at 5.0 μm (red) (Figure 5C and Supporting Information for the original data, Figures S5 and S6). The measurement was performed in negative ion mode, so the mass value reflected a sodium ion adduct (+23) of the *N*-acetylglucosamine residue (221 Da). The production yield of monomeric sugars was estimated to be several percent of the total eluates based on the peak intensity on the chromatogram.

https://doi.org/10.1021/acsomega.4c07531
ACS Omega 2025, 10, 13860−13867

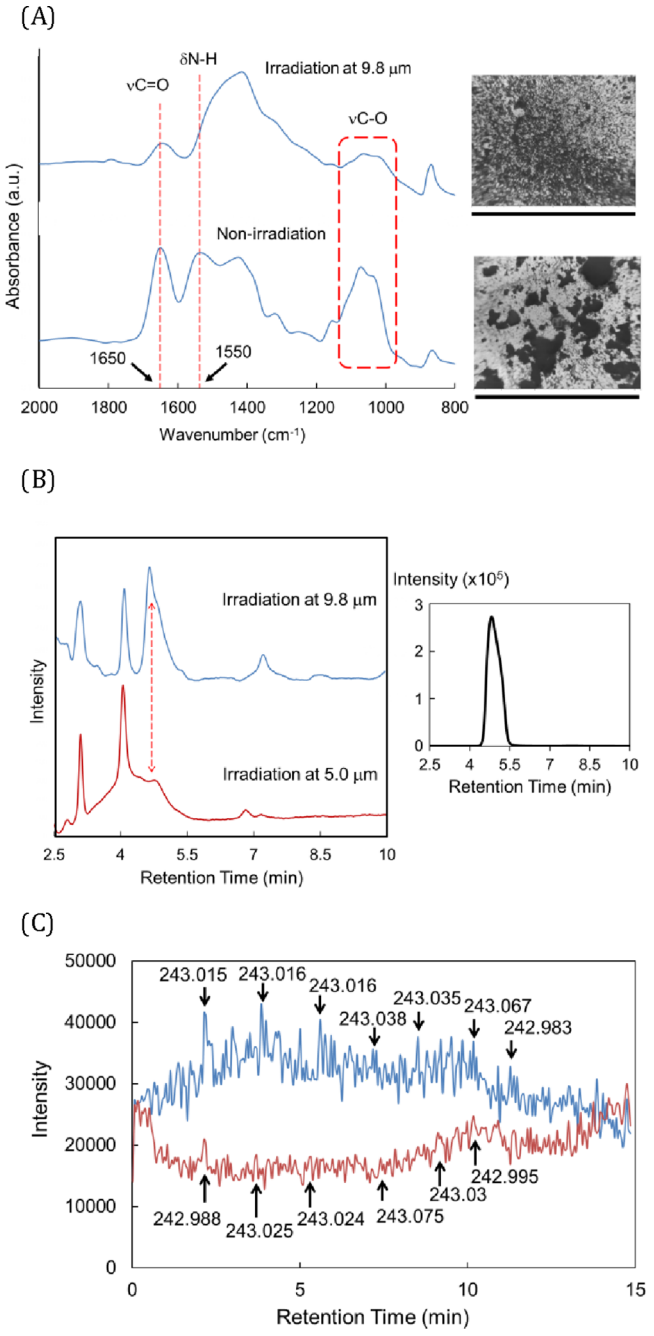

Figure 5. Irradiation effect of IR-FEL on outer shells of crayfish. (A) SR-IRM spectra of outer shell of crayfish before (bottom) and after irradiation at 9.8 μm (upper) from 800 to 2000 cm^{-1}. The photographs on the right show microscopic images of the measurement area on the sample surface. Black bar: 1 mm. (B) Liquid chromatography (LC) profiles of the outer shells of crayfish after IR-FEL irradiation (left panel) and *N*-acetyl glucosamine treatment alone (right panel). (C) ESI-MS chromatograms of 243 Da after irradiations at 9.8 μm (blue) and 5.0 μm (red).

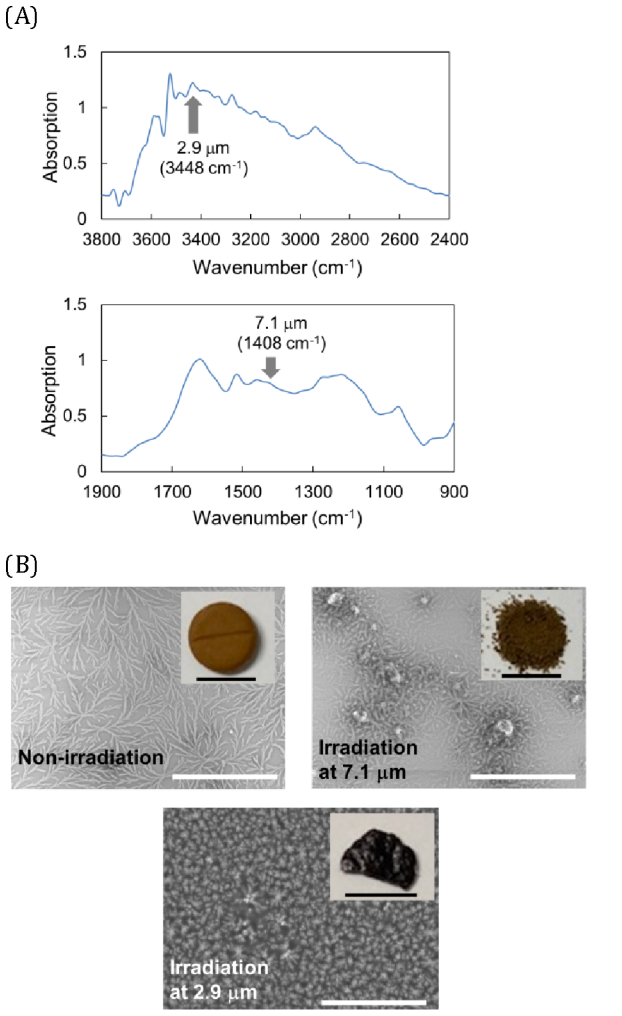

Figure 6. Effect of IR-FEL irradiation on SL. (A) SR-IRM spectra before irradiation at 900−1900 (bottom) and 2400−3800 cm^{-1} (upper). The gray arrows indicate the irradiation wavelengths. (B) SEM images before (upper left) and after irradiations at 7.1 (upper right) and 2.9 μm (below). The small photograph on the right edge of each image shows the optical microscopy image of the lignin sample. White bar: 30 μm; black bar: 1 cm.

Taken together, these results suggest that IR-FEL irradiation at 9.8 μm can degrade the chitin chains in the outer shell of crayfish, resulting in the release of the *N*-acetylglucosamine moiety.

3.2. Fragmentation of SL. The irradiation effect of the IR-FEL on the SL is also shown. We tested two wavelengths (Figure 6A): 2.9 μm (3448 cm^{-1}), resonant with the O−H stretching mode (νO−H); and 7.1 μm (1408 cm^{-1}), covering broad absorption bands including C−C stretching (νC−C) and H−C−O bending (δH−C−O) modes. The absorption intensities at both wavelengths were similar.

In the SEM and optical microscopy images (Figure 6B), the powder was light brown, and many tiny branches were assembled on the surface of the SL before irradiation (upper left). On the other hand, after irradiation at 2.9 μm (below), the powder transformed into a black and glutinous material, and the branch-like surface changed into small particles; irradiation at 7.1 μm destroyed only several parts, and the color change was unremarkable (upper right).

The structural change of SL induced by the O−H targeting irradiation at 2.9 μm was analyzed using THz-CER spectroscopy at 0.3−1.2 THz (Figure 7). The overall transmission in the sample irradiated at 7.1 μm (blue) and that before irradiation (black) are comparatively high. However, the transmittances at 0.33, 0.43, and 0.54 THz significantly decreased under 2.9 μm irradiation (red), while the overall spectral shape resembled that of the other samples. This

https://doi.org/10.1021/acsomega.4c07531
ACS Omega 2025, 10, 13860−13867

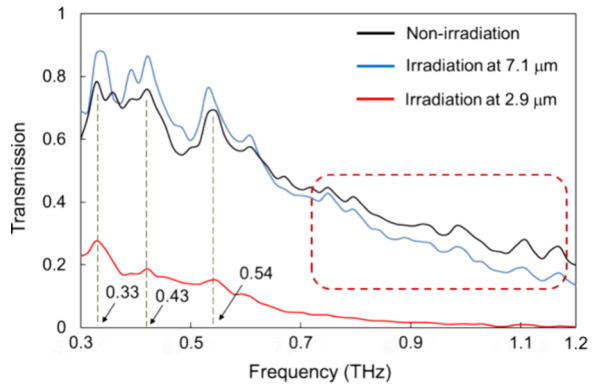

Figure 7. THz-CER spectra of SL from 0.3 to 1.2 THz before (black) and after irradiations at 7.1 (blue) and 2.9 μm (red).

indicates that the SL sample absorbed more THz waves after 2.9 μm irradiation than before irradiation.

In our previous study on the THz spectral measurement of a protein aggregate, we observed that the absorption intensity at ≈1.0 THz in the nonaggregate (native) protein was higher than that in the fibrous aggregate.[43] Therefore, the increase in the absorption of the THz wave indicates that the polymeric state of SL is dissociated by 2.9 μm irradiation, similar to the case of the disaggregation of protein fibrils. In the case of 7.1 μm irradiation, the reducing angle from 0.7 to 1.2 THz is slightly larger than that before irradiation (dotted square). This may be associated with a change in the refractive index of the lignin sample, as indicated by the morphological changes (Figure 6B).

The SR-IRM analysis results after irradiation are shown in Figure 8. In the mid-IR region (right panel), the shoulder peak

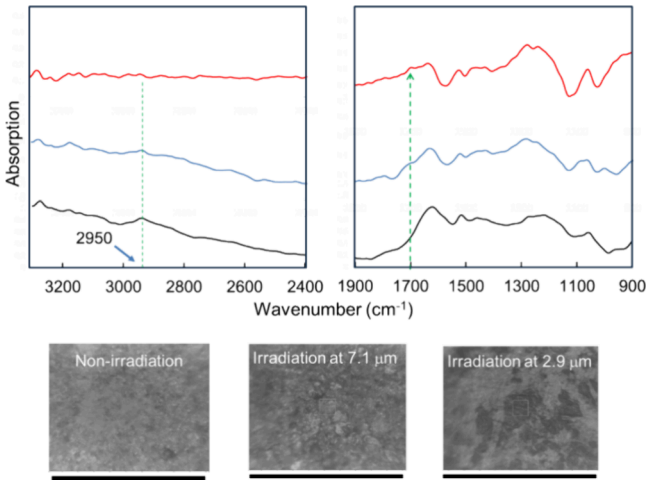

Figure 8. SR-IRM spectra of SL from 900 to 3300 cm^{-1} before (black) and after irradiations at 7.1 (blue) and 2.9 μm (red). Microscopy images of the measurement area of the sample surface are shown along the bottom. Black bar: 1 mm.

at 1700 cm^{-1} increased after irradiation at 2.9 μm (red) compared with that after 7.1 μm irradiation (blue) and no irradiation (black). This region contains the C = O stretching vibrational modes of the aldehyde and carboxyl groups. In the near-IR region (left panel), the absorption intensities from 2650 cm^{-1} to 3150 cm^{-1} significantly decreased, and the peak at 2950 cm^{-1} disappeared after irradiation at 2.9 μm (red) but remained in the spectra after 7.1 μm irradiation (blue) and no irradiation (black). This region contains O−H and C−H stretching modes in the main-chain backbone of lignin. In addition, the OH group in sulfonic acid was also observed. These spectral changes indicate a drastic deformation of the SL, accompanied by the release of compounds containing carbonyl and sulfonyl groups, which can be caused by irradiation at 2.9 μm.

In the ESI-MS spectrum range of 380 to 896 m/z (Figure 9A and Supporting Information for the original data, Figures S7–

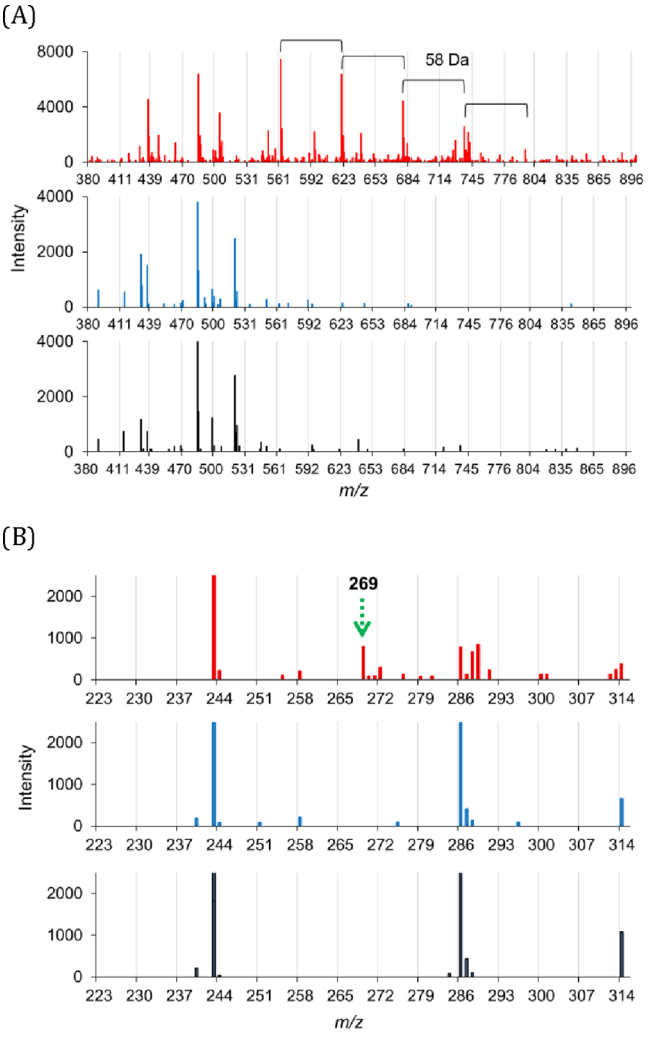

Figure 9. (A) ESI-MS profiles of SL in the high-molecular-weight range of 380–896 m/z before (black) and after irradiations at 7.1 μm (blue) and 2.9 μm (red). (B) ESI-MS profiles in the low-molecular-weight range of 223–314 m/z before (black) and after irradiations at 7.1 (blue) and 2.9 μm (red).

S9), multivalent ions are remarkably detected from 500 to 800 Da after irradiation at 2.9 μm (upper) but are not detected in the spectra of the nonirradiated sample (black) and the sample irradiated at 7.1 μm (blue). The interval of the multivalent ions was 58 Da, which was consistent with the $(C_2O_2H_2)^+$, $(C_3OH_6)^+$ or $(C_4H_{10})^+$ fragments. The lignin backbone is generally composed of hydroxyphenyl propane chains; therefore, the $(C_3OH_6)^+$ fragment is more likely to have the corresponding structure. This implies that the polymeric structure of SL was dissociated by irradiation at 2.9 μm,

https://doi.org/10.1021/acsomega.4c07531
ACS Omega 2025, 10, 13860−13867

producing many more fragment ions than the nonirradiated and 7.1 μm irradiated samples.

Below 300 Da (Figure 9B), a new peak at 269 Da (green arrow) appears after irradiation at 2.9 μm (top). This peak was detected neither after irradiation at 7.1 μm (middle) nor before irradiation (below). Detection was performed in the positive ion mode. As a possible candidate, this peak can be assigned to the sodium ion adduct (+23) of coniferyl aldehyde (178 Da) substituted with a sulfinate (SO_2H) group (65 Da) and two hydrogen atoms (+2). In the FT-IR spectra (Figure 8), the absorption intensities of the OH and CH groups decreased, and a new peak emerged at ≈1700 cm^{-1}, corresponding to the C = O stretching mode. The mass and IR data indicate that low-molecular-weight aromatic compounds containing aldehyde and sulfinate groups were released from the intact SL by VE of the O−H stretching mode.

4. DISCUSSION

Currently, the research and development of efficient strategies to recycle renewable resources into industrially useful materials are geared toward the realization of a sustainable society. In this study, we propose a physicochemical approach using an intense IR laser as a "molecular cutter" to decompose solid-state biomacromolecules using chitin and lignin as model samples. In the former case, the glycoside bonds were cleaved by laser irradiation targeting the C−O stretching vibrational mode (9.8 μm), and a functional sugar was obtained from the outer shells of crayfish. Considering the effect of irradiation on cellulose,[22] it can be ascertained that the VE of covalent bonds in the sugar−sugar linkage is effective in degrading polysaccharides into their monomeric sugars. A percentage of the *N*-acetyl glucosamine residue was released from the intact outer shell powder based on the peak intensity in the mass chromatogram. As the yield is not necessarily high under the current irradiation conditions at the laboratory level, the irradiation parameters (e.g., irradiation time and pulse energy) must be optimized to improve the degradation efficacy as a next step.

In the case of lignin degradation, we have previously shown that alkaline lignin prepared after the neutralization of sulfonated lignin can be degraded by IR-FEL.[23] In this case, vanillic acid was separated by irradiation at 7.1 μm. By contrast, the irradiation effect on sulfonated lignin at the same wavelength appeared to be slightly weaker than that at 2.9 μm. It can be considered that sulfonated lignin absorbs less VE energy (7.1 μm) than alkaline lignin. Rather, the effect of 2.9 μm irradiation on fragmentation was remarkable, and irradiation released the coniferyl aldehyde derivative. For alkaline lignin, coniferyl alcohol was obtained after irradiation at 2.9 μm in a similar manner.[23] Therefore, it seems likely that the VE of the stretching mode of the hydroxy group can be effective in decomposing the polymeric structure of lignin to produce low-molecular-weight coniferyl compounds.

In our IR-FEL application study, various biomacromolecules were degraded by mode-selective VE reactions. In general, natural biomacromolecules form molecular clusters constructed by noncovalent bonds, such as hydrogen bonds and covalent linkages of C−O and C−C bonds (Figure 10). These biomolecular clusters can be dissociated and fragmented into their monomeric conformations by inducing VEs at each specific IR absorption band. These VE reactions are unique in their use of a high-energy accelerator; traditional methods employ microbiome and enzyme catalysis to degrade

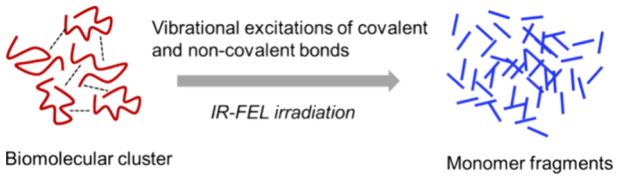

Figure 10. IR-FEL mediates the decomposition of biomolecular clusters into their monomeric forms. Biomolecular clusters were formed by covalent and noncovalent bonds (blue dotted lines). The aggregate structure can be dissociated into a nonaggregate state, and the covalent bonds can be cleaved to produce fragmented monomers by IR-FEL irradiation at specific absorption wavelengths.

biomolecules and organic macromolecules.[44−46] However, many organic molecules possess IR absorption bands (Figure 1), and the IR-FEL irradiation technique can be adopted to irradiate many types of organic materials by tuning their wavelengths to their specific vibrational modes.

To develop IR-FEL as a versatile analytical tool, it is important to investigate the effect of irradiation on real materials containing multiple components. Previously, we used IR-FEL to irradiate fossilized inks from cephalopods, which are composed of melanin, hydroxyapatite, calcium carbonate, and proteins.[47] As shown in that study, the structure of the sample is expected to change significantly if the irradiation wavelength resonates with the main functional group. If the structural damage is minor, it can be assumed that the number of chemical bonds corresponding to the irradiation wavelength can be reduced. Because irradiation wavelengths can be tuned by changing the gap length of the undulator (periodic magnetic field in the linear accelerator), an IR-FEL irradiation system was used to screen the wavelengths that resonated with the functional group within the target sample.

Given the versatility of IR radiation, future studies should examine the targeting of environmentally persistent and toxic organic chemicals. Nonetheless, it is necessary to develop compact and tabletop IR laser instruments equipped with both high photon density and wavelength tunability for the practical implementation of molecular VE reactions in the future. The IR-FEL system is currently installed at a synchrotron radiation facility, but it is too large for use by chemical recycling companies.

5. CONCLUSIONS

IR-FEL is an accelerator-based IR laser featuring wavelength tunability and high photon density. Isolated chitin, crayfish exoskeleton, and SL were irradiated by IR-FEL, and their structural changes were analyzed using SR-IRM, ESI-MS, SEM, and THz-CER. SR-IRM analyses showed that the glycoside bond in chitin was cleaved by irradiation at 9.8 μm, which resonates with the C−O stretching vibration (νC−O), and *N*-acetyl glucosamine was produced from the exoskeleton of crayfish by C−O-targeting irradiation, as shown in the ESI-MS spectra. Nonspecific irradiation at 5.0 μm (low absorption wavelength) had little effect on either the IR or mass spectra. The SEM images and THz-CER spectra showed that the aggregated state of SL dissociated into a nonaggregated state by irradiation at 2.9 μm, which is resonant with the O−H stretching vibrational mode; VE at 7.1 μm did not have the same effect. In addition, the main chain of lignin was fragmented, and the coniferyl aldehyde derivative was released by O−H-targeting irradiation, as evidenced by the SR-IRM and ESI-MS spectra. The decomposition reaction proceeded at

https://doi.org/10.1021/acsomega.4c07531
ACS Omega 2025, 10, 13860−13867

room temperature in the absence of solvent. The IR-FEL system is a promising tool for analyzing a variety of solid-state biomacromolecules.

■ ASSOCIATED CONTENT

Supporting Information

The Supporting Information is available free of charge at https://pubs.acs.org/doi/10.1021/acsomega.4c07531.

IR-FEL oscillation system, THz-CER spectroscopy, and ESI-MS data (PDF)

■ AUTHOR INFORMATION

Corresponding Author

Takayasu Kawasaki − *Accelerator Laboratory, High Energy Accelerator Research Organization, Tsukuba, Ibaraki 305-0801, Japan*; orcid.org/0000-0001-8376-5807; Email: takayasu.kawasaki@kek.jp

Authors

Atsushi Nagase − *Laboratory for Electron Beam Research and Application (LEBRA), Institute of Quantum Science, Nihon University, Funabashi, Chiba 274-8501, Japan*

Ken Hayakawa − *Laboratory for Electron Beam Research and Application (LEBRA), Institute of Quantum Science, Nihon University, Funabashi, Chiba 274-8501, Japan*

Fumitsuna Teshima − *National Institutes of Natural Sciences Institute for Molecular Science, UVSOR Synchrotron Facility, Okazaki, Aichi 444-8585, Japan*

Kiyohisa Tanaka − *National Institutes of Natural Sciences Institute for Molecular Science, UVSOR Synchrotron Facility, Okazaki, Aichi 444-8585, Japan*

Heishun Zen − *Institute of Advanced Energy, Kyoto University, Uji, Kyoto 611-0011, Japan*

Fumio Shishikura − *Laboratory for Electron Beam Research and Application (LEBRA), Institute of Quantum Science, Nihon University, Funabashi, Chiba 274-8501, Japan*

Norihiro Sei − *Research Institute for Measurement and Analytical Instrumentation, National Institute of Advanced Industrial Science and Technology, Tsukuba, Ibaraki 305-8568, Japan*

Takeshi Sakai − *Laboratory for Electron Beam Research and Application (LEBRA), Institute of Quantum Science, Nihon University, Funabashi, Chiba 274-8501, Japan*

Yasushi Hayakawa − *Laboratory for Electron Beam Research and Application (LEBRA), Institute of Quantum Science, Nihon University, Funabashi, Chiba 274-8501, Japan*

Complete contact information is available at: https://pubs.acs.org/10.1021/acsomega.4c07531

Notes

The authors declare no competing financial interest.

■ ACKNOWLEDGMENTS

This research was supported by the TIA collaborative research program "Kakehashi" (TK23-007 and TK22-050) and the grant from The Yanmar Environmental Sustainability Support Association (grant number: 2). Part of this work was supported by the Advanced Research Infrastructure for Materials and Nanotechnology in Japan (ARIM) of the Ministry of Education, Culture, Sports, Science, and Technology (MEXT) under project issue number 23 NM0121. We thank Dr. Shinya Hattori for technical assistance with ESI-MS. Part of this research was performed at the BL6B of the UVSOR Synchrotron Facility, Institute for Molecular Science (IMS programs 23IMS6662 and 23IMS6845) and was partly conducted through collaborative research with LEBRA at Nihon University and the Joint Usage/Research Program on Zero-Emission Energy Research, Institute of Advanced Energy, Kyoto University (ZE2022A-15 and ZE2023A-20). We thank Mr. Masaki Ishida for technical support with SEM and optical microscopy.

■ ABBREVIATIONS

IR-FEL, infrared free-electron laser; SR-IRM, synchrotron radiation infrared microscopy; ESI-MS, electrospray ionization mass spectroscopy; THz-CER, terahertz coherent edge radiation; SEM, scanning electron microscopy; SL, sulfonated lignin

■ REFERENCES

(1) Edwards, N. P.; Barden, H. E.; van Dongen, B. E.; Manning, P. L.; Larson, P. L.; Bergmann, U.; Sellers, W. I.; Wogelius, R. A. Infrared mapping resolves soft tissue preservation in 50 million year-old reptile skin. *Proc. Biol. Sci.* **2011**, *278* (1722), 3209−18.

(2) Song, C.; Fan, W. H.; Ding, L.; Chen, X.; Chen, Z. Y.; Wang, K. Terahertz and infrared characteristic absorption spectra of aqueous glucose and fructose solutions. *Sci. Rep.* **2018**, *8* (1), 8964.

(3) Mann, D.; Höweler, U.; Kötting, C.; Gerwert, K. Elucidation of Single Hydrogen Bonds in GTPases via Experimental and Theoretical Infrared Spectroscopy. *Biophys. J.* **2017**, *112* (1), 66−77.

(4) Meizyte, G.; Brown, R. H.; Brewer, E. I.; Watson, P. D.; Mackenzie, S. R. A Combined Infrared and Computational Study of Gas-Phase Mixed-Ligand Rhodium Complexes: Rh(CO)n(N2O)m+ (n = 1−5, m = 1−4). *J. Phys. Chem. A* **2023**, *127* (44), 9220−9228.

(5) Wang, H.; Seemakurthi, R. R.; Chen, G. F.; Strauss, V.; Savateev, O.; Hai, G.; Ding, L.; López, N.; Wang, H.; Antonietti, M. Laser-induced nitrogen fixation. *Nat. Commun.* **2023**, *14* (1), 5668.

(6) Greisch, J. F.; van der Laarse, S. A. M.; Heck, A. J. R. Enhancing Top-Down Analysis Using Chromophore-Assisted Infrared Multiphoton Dissociation from (Phospho)peptides to Protein Assemblies. *Anal. Chem.* **2020**, *92* (23), 15506−15516.

(7) Peters-Clarke, T. M.; Schauer, K. L.; Riley, N. M.; Lodge, J. M.; Westphall, M. S.; Coon, J. J. Optical Fiber-Enabled Photoactivation of Peptides and Proteins. *Anal. Chem.* **2020**, *92* (18), 12363−12370.

(8) Munshi, M. U.; Berden, G.; Oomens, J. Infrared Ion Spectroscopic Characterization of the Gaseous [Co(15-crown-5)-(H2O)]2+ Complex. *J. Phys. Chem. A* **2023**, *127* (34), 7256−7263.

(9) Smith, Z. M.; Steinmetz, V.; Martens, J.; Oomens, J.; Poutsma, J. C. Infrared Multiple Photon Dissociation Spectroscopy of Cationized Canavanine: Side-Chain Substitution Influences Gas-Phase Zwitterion Formation. *Int. J. Mass Spectrom.* **2018**, *429*, 158−173.

(10) Glotin, F.; Chaput, R.; Jaroszynski, D.; Prazeres, R.; Ortega, J.-M. Infrared subpicosecond laser pulses with a free-electron laser. *Phys. Rev. Lett.* **1993**, *71*, 2587−2590.

(11) Grosse, E. THz radiation from free electron lasers and its potential for cell and tissue studies. *Phys. Med. Biol.* **2002**, *47*, 3755−3760.

(12) Vogel, A.; Venugopalan, V. Mechanisms of Pulsed Laser Ablation of Biological Tissues. *Chem. Rev.* **2003**, *103*, 577−644.

(13) Ovelmen-Levitt, J.; Straub, K. D.; Hauger, S.; Szarmes, E.; Madey, J.; Pearlstein, R. D.; Nashold, B. S., Jr. Brain ablation in the rat cerebral cortex using a tunable-free electron laser. *Lasers Surg. Med.* **2003**, *33*, 81−92.

(14) Austin, R. H.; Xie, A.; van der Meer, L.; Redlich, B.; Lindgård, P.-A.; Frauenfelder, H.; Fu, D. Picosecond Thermometer in the Amide I Band of Myoglobin. *Phys. Rev. Lett.* **2005**, *94*, No. 128101.

(15) Zavalin, A.; Hachey, D. L.; Sundaramoorthy, M.; Banerjee, S.; Morgan, S.; Feldman, L.; Tolk, N.; Piston, D. W. Kinetics of a

Collagen-Like Polypeptide Fragmentation after Mid-IR Free-Electron Laser Ablation. *Biophys. J.* **2008**, *95*, 1371−1381.
(16) Andersson, Å.; Poline, M.; Kodambattil, M.; Rebrov, O.; Loire, E.; Maître, P.; Zhaunerchyk, V. Structure of Proton-Bound Methionine and Tryptophan Dimers in the Gas Phase Investigated with IRMPD Spectroscopy and Quantum Chemical Calculations. *J. Phys. Chem. A* **2020**, *124*, 2408−2415.
(17) Munshi, M. U.; Martens, J.; Berden, G.; Oomens, J. Protoisomerization of Indigo and Isoindigo Dyes Confirmed by Gas-Phase. Infrared Ion Spectroscopy. *J. Phys. Chem. A* **2019**, *123*, 8226−8233.
(18) Irizawa, A.; Fujimoto, M.; Kawase, K.; Kato, R.; Fujiwara, H.; Higashiya, A.; Macis, S.; Tomarchio, L.; Lupi, S.; Marcelli, A.; et al. Spatially Resolved Spectral Imaging by A THz-FEL. *Condens. Matter* **2020**, *5*, 38.
(19) Halliwell, D. E.; Morais, C. L.; Lima, K. M.; Trevisan, J.; Siggel-King, M. R.; Craig, T.; Ingham, J.; Martin, D. S.; Heys, K.; Kyrgiou, M.; et al. An imaging dataset of cervical cells using scanning near-field optical microscopy coupled to an infrared free electron laser. *Sci. Data* **2017**, *4*, No. 170084.
(20) Kawasaki, T.; Man, V. H.; Sugimoto, Y.; Sugiyama, N.; Yamamoto, H.; Tsukiyama, K.; Wang, J.; Derreumaux, P.; Nguyen, P. H. Infrared Laser-Induced Amyloid Fibril Dissociation: A Joint Experimental/Theoretical Study on the GNNQQNY Peptide. *J. Phys. Chem. B* **2020**, *124*, 6266−6277.
(21) Kawasaki, T.; Sato, A.; Tominaga, Y.; Suzuki, Y.; Oyama, T.; Tadokoro, M.; Tsukiyama, K.; Nokihara, K.; Zen, H. Photo-Modification of Melanin by a Mid-Infrared Free-Electron Laser. *Photochem. Photobiol.* **2019**, *95*, 946−950.
(22) Kawasaki, T.; Sakai, T.; Zen, H.; Sumitomo, Y.; Nogami, K.; Hayakawa, K.; Yaji, T.; Ohta, T.; Tsukiyama, K.; Hayakawa, Y. Cellulose Degradation by Infrared Free Electron Laser. *Energy Fuels* **2020**, *34*, 9064−9068.
(23) Kawasaki, T.; Zen, H.; Sakai, T.; Sumitomo, Y.; Nogami, K.; Hayakawa, K.; Yaji, T.; Ohta, T.; Nagata, T.; Hayakawa, Y. Degradation of Lignin by Infrared Free Electron Laser. *Polymers* **2022**, *14*, 2401.
(24) Rkhaila, A.; Chtouki, T.; Erguig, H.; El Haloui, N.; Ounine, K. Chemical Proprieties of Biopolymers (Chitin/Chitosan) and Their Synergic Effects with Endophytic Bacillus Species: Unlimited Applications in Agriculture. *Molecules* **2021**, *26* (4), 1117.
(25) Bai, L.; Liu, L.; Esquivel, M.; Tardy, B. L.; Huan, S.; Niu, X.; Liu, S.; Yang, G.; Fan, Y.; Rojas, O. J. Nanochitin: Chemistry, Structure, Assembly, and Applications. *Chem. Rev.* **2022**, *122* (13), 11604−11674.
(26) Wibowo, E. S.; Park, B. D. Chemical and Thermal Characteristics of Ion-Exchanged Lignosulfonate. *Molecules.* **2023**, *28* (6), 2755.
(27) Aro, T.; Fatehi, P. Production and Application of Lignosulfonates and Sulfonated Lignin. *ChemSusChem.* **2017**, *10* (9), 1861−1877.
(28) Wang, X.; Isbrandt, T.; Strube, M. L.; Paulsen, S. S.; Nielsen, M. W.; Buijs, Y.; Schoof, E. M.; Larsen, T. O.; Gram, L.; Zhang, S. D. Chitin Degradation Machinery and Secondary Metabolite Profiles in the Marine Bacterium Pseudoalteromonas rubra S4059. *Mar Drugs.* **2021**, *19* (2), 108.
(29) Raimundo, I.; Silva, R.; Meunier, L.; Valente, S. M.; Lago-Lestón, A.; Keller-Costa, T.; Costa, R. Functional metagenomics reveals differential chitin degradation and utilization features across free-living and host-associated marine microbiomes. *Microbiome.* **2021**, *9* (1), 43.
(30) Oyeleye, A.; Normi, Y. M. Chitinase: diversity, limitations, and trends in engineering for suitable applications. *Biosci Rep.* **2018**, *38* (4), BSR2018032300.
(31) Janusz, G.; Pawlik, A.; Sulej, J.; Swiderska-Burek, U.; Jarosz-Wilkolazka, A.; Paszczynski, A. Lignin degradation: microorganisms, enzymes involved, genomes analysis and evolution. *FEMS Microbiol Rev.* **2017**, *41* (6), 941−962.
(32) Silva, J. P.; Ticona, A. R. P.; Hamann, P. R. V.; Quirino, B. F.; Noronha, E. F. Deconstruction of Lignin: From Enzymes to Microorganisms. *Molecules.* **2021**, *26* (8), 2299.
(33) Fernandes, M. R. C.; Huang, X.; Abbenhuis, H. C. L.; Hensen, E. J. M. Lignin oxidation with an organic peroxide and subsequent aromatic ring opening. *Int. J. Biol. Macromol.* **2019**, *123*, 1044−1051.
(34) Dier, T. K. F.; Rauber, D.; Durneata, D.; Hempelmann, R.; Volmer, D. A. Sustainable Electrochemical Depolymerization of Lignin in Reusable Ionic Liquids. *Sci. Rep.* **2017**, *7* (1), 5041.
(35) Zen, H.; Hajima, R.; Ohgaki, H. Full characterization of superradiant pulses generated from a free-electron laser oscillator. *Sci. Rep.* **2023**, *13*, 6350.
(36) Zen, H.; Suphakul, S.; Kii, T.; Masuda, K.; Ohgaki, H. Present status and perspectives of long wavelength free electron lasers at Kyoto University. *Phys. Procedia* **2016**, *84*, 47−53.
(37) Nakao, K.; Hayakawa, K.; Hayakawa, Y.; Inagaki, M.; Nogami, K.; Sakai, T.; Tanaka, T.; Zen, H. Pulse Structure Measurement of Near-Infrared FEL in Burst-Mode Operation of LEBRA Linac. In *Proceedings of FEL2012*; Nara, Japan, 2012, p 472.
(38) Hayakawa, Y.; Sato, I.; Hayakawa, K.; Tanaka, T.; et al. First lasing of LEBRA FEL at Nihon University at a wavelength of 1.5 μm. *Nucl. Instrum. Methods Phys. Res. A* **2002**, *483*, 29−33.
(39) Kimura, S.; et al. Infrared and terahertz spectromicroscopy beam line BL6B(IR) at UVSOR-II. *Infrared Phys. Technol.* **2006**, *49*, 147−151.
(40) Sei, N.; Ogawa, H.; Hayakawa, K.; Tanaka, T.; Hayakawa, Y.; Nakao, K.; Sakai, T.; Nogami, K.; Inagaki, M. Observation of intense terahertz-wave coherent synchrotron radiation at LEBRA. *J. Phys. D: Appl. Phys.* **2013**, *46*, No. 045104.
(41) Sei, N.; Ogawa, H.; Sakai, T.; Hayakawa, K.; Tanaka, T.; Hayakawa, Y.; Nogami, K. Millijoule terahertz coherent transition radiation at LEBRA. *Jpn. J. Appl. Phys.* **2017**, *56*, No. 032401.
(42) Sei, N.; Ogawa, H.; Sakai, T.; Sumitomo, Y.; Hayakawa, Y.; Takahashi, Y.; Nogami, K.; Tanaka, T.; Hayakawa, K. Terahertz-wave Beamline Using Coherent Edge Radiation at Nihon University. In *2022 Conference on Lasers and Electro-Optics Pacific Rim (CLEO-PR)*; IEEE: 2022. DOI: .
(43) Kawasaki, T.; Izumi, Y.; Ohori, G.; et al. Study on Irradiation Effect of Mid-Infrared Free Electron Laser on Hen Egg-White Lysozyme by Using Terahertz-Time Domain Spectroscopy and Synchrotron-Radiation Vacuum-Ultraviolet Circular-Dichroism Spectroscopy. *J. Infrared Milli. Terahz. Waves* **2019**, *40*, 998−1009.
(44) Lynd, L. R.; Weimer, P. J.; van Zyl, W. H.; Pretorius, I. S. Microbial cellulose utilization: fundamentals and biotechnology. *Microbiol Mol. Biol. Rev.* **2002**, *66* (3), 506−77.
(45) Wang, X.; Yao, B.; Su, X. Linking Enzymatic Oxidative Degradation of Lignin to Organics Detoxification. *Int. J. Mol. Sci.* **2018**, *19* (11), 3373.
(46) Unuofin, J. O.; Odeniyi, O. A.; Majengbasan, O. S.; Igwaran, A.; Moloantoa, K. M.; Khetsha, Z. P.; Iwarere, S. A.; Daramola, M. O. Chitinases: expanding the boundaries of knowledge beyond routinized chitin degradation. *Environ. Sci. Pollut Res. Int.* **2024**, *31* (26), 38045−38060.
(47) Kawasaki, T.; Zen, H.; Ozaki, K.; Yamada, H.; Wakamatsu, K.; Ito, S. Application of mid-infrared free-electron laser for structural analysis of biological materials. *J. Synchrotron Rad.* **2021**, *28*, 28−35.

https://doi.org/10.1021/acsomega.4c07531
ACS Omega 2025, 10, 13860−13867